Critical conductivity ratio for conjugate heat transfer in eccentric annuli

M.A.I. El-Shaarawi and S.A. Haider
Mechanical Engineering Department, King Fahd University of Petroleum & Minerals, Dhahran, Saudi Arabia

Received May 2000
Revised January 2001
Accepted January 2001

Keywords *Forced convection, Heat transfer, Annuli*

Abstract *Conjugate laminar forced convection heat transfer in the entry region of eccentric annuli is numerically investigated. Heat transfer parameters are presented for a fluid of Pr = 0.7 flowing in an annulus of radius ratio 0.5 for four values of dimensionless eccentricity ranging from 0.1 to 0.7. Solid-fluid conductivity ratio (KR) is varied to cover the range for practical cases with commonly encountered inner and outer tube thickness. Boundary conditions applied are isothermal heating of the inner surface of the core tube, while the outer surface of the external tube is maintained at the inlet fluid temperature. Limits for KR above which the conjugation can be neglected are obtained.*

Nomenclature

$\dot{a}$ = location of the positive pole of the bipolar coordinate system on the x-axis, equal r_{oi} Sinh η_i or r_{io} Sinh η_o
D_h = hydraulic diameter of annulus, 2 ($r_{io} - r_{oi}$)
e = eccentricity (distance between axes of the two tubes), a (Coth η_o-Coth (η_i)
E = dimensionless eccentricity, e/(r_{io}-r_{oi}) $= \frac{\mathrm{Sinh}(\eta_i - \eta_o}{\mathrm{Sinh}\eta_i - \mathit{Sinh}\eta_o}$
h = coordinate transformation scale factor
H = dimensionless coordinate transformation scale factor, $h/D_h = \frac{0.5\sinh(\eta_o)}{(1-NR_2)(\cosh(\eta)-\cos(\zeta))}$
i = index for the bipolar grid in the η-direction and the cylindrical grid in the radial direction
j = index for the bipolar grid in the ζ-direction and the cylindrical grid in the tangential direction
k_f = thermal conductivity of fluid
k_s = thermal conductivity of solid
KR = solid-fluid conductivity ratio, k_s/k_f
M = number of intervals in the ζ and ϕ-directions
N = number of intervals in the η-direction
NR_1 = radius ratio, r_{ii}/r_{io}
NR_2 = radius ratio, r_{oi}/r_{io}
NR_4 = radius ratio, r_{oo}/r_{io}
NSI = number of radial intervals in the inner tube wall
NSO = number of radial intervals in the outer tube wall
Pr = Prandtl number for fluid, μ Cp/k_f
Q_{II} = average heat flux on the inner interface
r = first transverse cylindrical coordinate
r_{ii} = inner radius of core tube
r_{oi} = outer radius of core tube
r_{io} = inner radius of external tube
r_{oo} = outer radius of external tube
R = dimensionless radial coordinate, r/r_{io}
T = temperature at any point
T_m = bulk temperature at any cross-section
T_o = ambient or entrance temperature
T_w = isothermal temperature of heated wall
u = axial velocity component
u_{avg} = average (mean) axial velocity
u_{fd} = fully-developed axial velocity component
U = dimensionless axial velocity, u/u_{avg}

The support of King Fahd University of Petroleum & Minerals to carry out this investigation is gratefully acknowledged.

U_{fd} = dimensionless fully developed axial velocity u_{fd}/u_{avg}
v = η-direction velocity component
V = dimensionless η-velocity component, vD_h/ν
w = ζ-direction velocity component
W = dimensionless ζ-velocity component, wD_h/ν
x = first transverse direction in the Cartesian coordinate system
y = second transverse direction in the Cartesian coordinate system
z = axial coordinate measured from the annulus entrance
Z = dimensionless axial coordinate, z/(Dh Re)
Z* = dimensionless axial coordinate, z/(Dh Re Pr)

Greek letters

ΔR = numerical grid mesh size in R-direction
$\Delta\zeta$ = numerical grid mesh size in the ζ-direction
$\Delta\eta$ = numerical grid mesh size in the η-direction
$\Delta\phi$ = numerical grid mesh size in the ϕ-direction
ζ = second transverse bipolar coordinate, related to the Cartesian coordinate y by;

$$y = \frac{a\,\mathrm{Sin}(\xi)}{\mathrm{Cosh}(\eta) - \mathrm{Cos}(\xi)}$$

η = first transverse bipolar coordinate, related to the Cartesian coordinate x by:

$$x = \frac{a\,\mathrm{Sinh}(\eta)}{\mathrm{Cosh}(\eta) - \mathrm{Cos}(\xi)}$$

η_i = value of η on the inner interface,

$$\log_e\left[\frac{N(1+E^2)+(1-E^2)}{2NE} + \sqrt{\left(\frac{N(1+E^2)+(1-E^2)}{2NE}\right)^2 - 1}\right] = \mathrm{Cosh}^{-1}\left[\frac{N(1+E^2)+(1-E^2)}{2NE}\right]$$

η_o = value of η on the outer interface,

$$\log_e\left[\frac{N(1-E^2)+(1+E^2)}{2E} + \sqrt{\left(\frac{N(1-E^2)+(1+E^2))^2}{2E} - 1\right}\right] = \mathrm{Cosh}^{-1}\left[\frac{N(1-E^2)+(1+E^2)}{2E}\right]$$

θ = dimensionless temperature, $(T-T_o)/(T_w-T_o)$
θ_{fd} = fully developed value of θ
ν = kinematic viscosity of fluid

Introduction

Analysis of fluid flow and heat transfer in eccentric annuli provides a useful model for many practical applications. Practical examples of forced convection in annuli include flow and heat transfer in double-pipe heat exchangers, nuclear fuel element cooling systems, absorber and glass envelope assembly in parabolic-cylindrical solar collectors. Manufacturing tolerances and/or the assembly process or the operating conditions lead to eccentricity. Also, since eccentricity results in an increase in heat transfer and a simultaneous decrease in the pressure drop (El-Shaarawi *et al.*, 1997), it can be intentionally provided to achieve enhanced performance of heat exchange equipment.

In conventional heat transfer analyses, it is common practice to prescribe the temperature or the heat flux at the fluid wall interface. Consequently, the energy equation for the fluid alone has to be solved. The results thus obtained are good only for heat transfer in flows bounded by walls having extremely small thermal resistance, i.e. very high thermal conductivity and/or very small thickness.

However, in actual practice, the wall thermal resistance is finite and the thermal conditions at the fluid-wall interface are different from their counterparts imposed at the other surface of the solid walls. Thus, the thermal conditions at the fluid-wall interface, which are not known a priori, depend on the thermal properties and flow characteristics of the fluid as well as the dimensions and properties of the solid wall. Such type of problems, where heat conduction in the solid is coupled with convective heat transfer, are often referred to as the conjugate problem. If the bounding cylinder walls are thick and have low thermal conductivity, the heat transfer can be significantly affected and conjugation (i.e. coupling of conduction and convection) must be taken into account.

A thorough review of the literature reveals that a solution for the problem of conjugate forced convection heat transfer in eccentric annuli has not been reported. The following paragraphs focus on the available literature pertaining to forced flow and heat transfer in eccentric annuli and conjugate heat transfer in tubes, parallel plate channels and concentric annuli.

Using the bipolar coordinates, Caldwell (1930) and Piercy *et al.* (1933) showed that the MacDonald's equation for the torsion moment is comparable with the equation for the volumetric flow rate of a fully developed forced laminar flow through an eccentric annulus. Snyder and Goldstein (1965) obtained the velocity distribution for the fully developed forced laminar flow through eccentric annuli. Redberger and Charles (1962) numerically solved the same problem using the bipolar coordinates. The differential equation was replaced by a finite-difference representation and an iterative method was used to solve the resultant set of algebraic equations. Cheng and Hwang (1968) obtained a solution for the energy equation in cylindrical coordinates for the fully developed laminar forced convection in eccentric annular ducts with heat sources and constant wall temperature gradient.

Using the method introduced by Cheng and Hwang (1968), Trombetta (1972) obtained an approximate analytical solution for the energy equation in cylindrical coordinates for the hydrodynamically and thermally fully developed forced convection in eccentric annuli under other thermal boundary conditions. Fully developed forced convection in eccentric annuli has been treated numerically by Suzuki *et al.* (1990). The finite-difference equivalents of the governing equations of velocity and temperature fields written in bipolar coordinates were solved using an iterative procedure. Sathymurthy *et al.* (1992) presented a numerical study for fully developed laminar mixed convection in vertical eccentric annular ducts. They solved the equations governing the velocity and temperature using a body conforming grid and finite volume technique.

Feldman *et al.* (1982a; 1982b) studied the hydrodynamic and thermal entry region for forced convection in eccentric annuli. The absence of axisymmetry gives rise to three velocity components in this entrance region. They simplified the hydrodynamic problem by using only two governing equations (the continuity and the axial momentum equation); the two transverse momentum equations were dropped. To complete their hydrodynamic model, they developed an additional relation between the two transverse velocity components.

El-Shaarawi *et al.* (1998) presented a boundary-layer model describing the laminar forced convection heat transfer in the entry region of eccentric annuli and a finite-difference numerical algorithm was developed for solving this model. The main objective was to introduce a mathematically well-posed model, i.e. a model capable of describing the forced flow and convection heat transfer without the need of assumptions dependent on prior knowledge of the mechanism of transverse flows in the entry region. Numerical results were presented for the developing velocity profiles and the pressure drop in annuli of radius ratio 0.5 and 0.9 with dimensionless eccentricity ranging from 0.1 to 0.8. Heat transfer parameters were tabulated for a fluid of Pr = 0.7 with the boundary conditions of an isothermally heated inner wall and an outer wall maintained at the inlet fluid temperature.

Literature up to 1976, related to conjugate heat transfer in ducts of various geometrical shapes, has been reviewed by Shah and London (1978). Mori *et al.* (1978; 1979) considered the problem of steady conjugate heat transfer with fully developed laminar flow between parallel plates when there is internal heat generation in the fluid. Using the finite-difference method, Faghri and Sparrow (1980) solved the steady conjugate heat transfer with hydrodynamically fully developed laminar flow in a thick-walled circular tube. Pagliarini (1991) considered the same problem with the exception that the flow is hydrodynamically developing. Sakakibara *et al.* (1987) analytically investigated the steady conjugate heat transfer problem in an annulus with a heated core and an insulated outside tube when the laminar flow is hydrodynamically fully developed.

Using LaPlace transform techniques, Kirshan (1983) analytically solved the transient conjugate problem for hydrodynamically and thermally fully developed laminar pipe flow with viscous dissipation. Olek *et al.* (1991) considered the same problem by means of a method of separation of variables and concluded that the degree of conjugation and viscous dissipation may have a great impact on the temperature distribution in the fluid.

The present work aims at obtaining a solution for the conjugate laminar forced convection heat transfer in the entry region of eccentric annuli. A solution for this problem has not been reported in the literature. The results of this investigation give the limiting values for the solid-fluid conductivity ratio, under which the conjugation should not be neglected for practical purposes.

Governing equations

Figure 1(a) shows a two-dimensional cross-section for the geometry of the problem under consideration. The axes of the two eccentric cylinders are perpendicular to the plane of the paper. Fluid is forced to flow axially in the annular space between the two eccentric cylinders. This eccentric geometry can easily be described by the bipolar coordinate system (η, ξ and z) shown in Figure 1(b). The transformation equations from the Cartesian coordinate system (x, y and z) to this bipolar system are given in the nomenclature. In this orthogonal coordinate system the two cylindrical boundaries of the fluid annulus coincide with two surfaces having constant values of η (η_i and η_o,

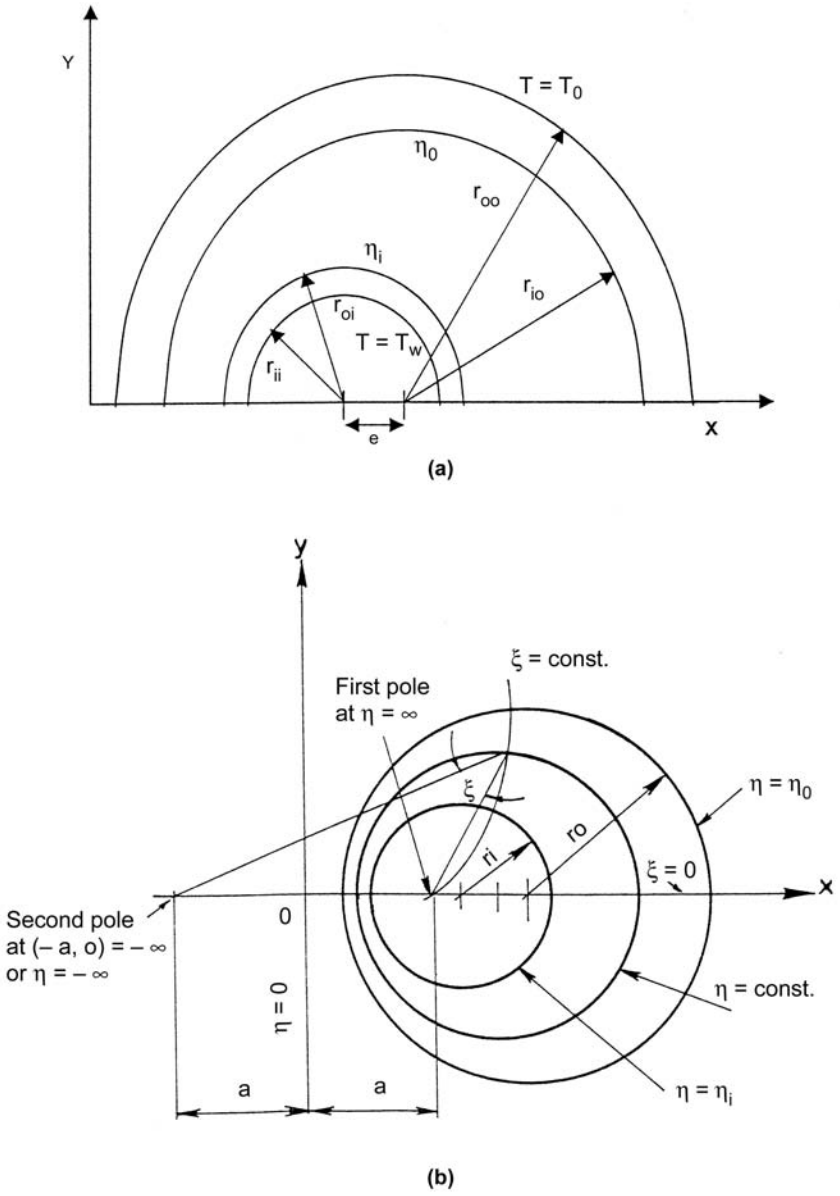

Figure 1.
(a) Two-dimensional cross-section of the geometry under consideration. (b) The bipolar coordinate system

which can be expressed in terms of the annulus radius ratio N and the dimensionless eccentricity E as given in the nomenclature). The other coordinate (ξ) represents a set of eccentric cylinders whose centers lie on the y-axis and which intersect orthogonally the boundaries of the fluid annulus. The transformed geometry for the fluid annulus in the complex $\eta - \xi$ plane is a slab of length ($\eta_i - \eta_o$) and width equal to the limits of ξ, that is 2π.

The present work aims at obtaining a solution for the conjugate heat transfer problem with laminar forced convection in the entry region of the eccentric annulus. The bipolar coordinate system is used to express the partial differential equations describing the flow and heat transfer in the eccentric fluid annulus. In this bipolar coordinate system the boundary surfaces of the fluid annulus are taken as one of the coordinates and the other coordinate comprises a set of eccentric cylinders that orthogonally intersect these boundaries. However, since the cylinder walls have uniform thickness, the cylindrical coordinate system is more appropriate for the solid walls. Therefore, the energy equation for each of the solid cylinder walls is expressed in cylindrical coordinates. Continuity of temperature and heat flux at the solid-fluid interfaces provides the necessary link. Figure 2 illustrates the numerical meshes, with a bipolar grid in the fluid annulus and cylindrical grids in the two solid walls.

The flow is assumed to besteady and the fluid is Newtonian with constant properties. Body forces, viscous dissipation, internal heat generation and radiation heat transfer are all absent. Axial diffusion of momentum in the fluid and that of energy in both the fluid and the solid are neglected. Pressure is a function of the axial coordinate only and momentum equation in the η-direction (i.e. the radial-like direction) is dropped, since the η-velocity component (v) is much smaller than the ζ- and z-velocity components (w and u, respectively).

Under these assumptions and using the following dimensionless parameters: $H = h/D_h$, $KR = k_s/k_f$, $NR_1 = r_{ii}/r_{io}$, $NR_2 = r_{oi}/r_{io}$, $NR_4 = r_{oo}/r_{io}$, $R = r/r_{io}$, $U = u/u_{avg}$, $V = v\ D_h/\nu$, $W = w\ D_h/\nu$, $Z = z/(D_h\ Re)$, $\theta = (T-T_o)/(T_w-T_o)$, we obtain the following six dimensionless equations:

Continuity equation

$$\frac{\partial(HW)}{\partial\zeta} + \frac{\partial(HV)}{\partial\eta} + \frac{\partial(H^2U)}{\partial Z} = 0 \tag{1}$$

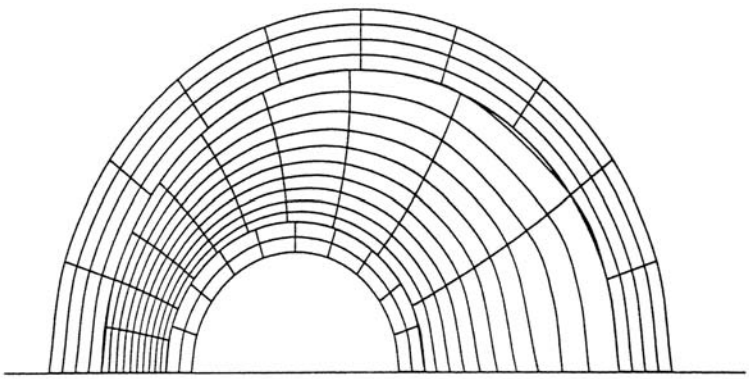

Figure 2.
Sample of the numerical grid mesh for N = M = 10, NSO = 4 and NSI = 2; computations were done using a mesh with N = M = 20; NSO = 16 and NSI = 8

ζ-Momentum equation

$$\frac{W}{H}\frac{\partial W}{\partial \zeta}+\frac{V}{H^2}\frac{\partial HW}{\partial \eta}+U\frac{\partial W}{\partial Z}-\frac{V^2}{H^2}\frac{\partial H}{\partial \zeta}$$
$$=\frac{1}{H^3}\left(\frac{\partial^2 HW}{\partial \eta^2}+\frac{\partial^2 HW}{\partial \zeta^2}\right)-\frac{2}{H^4}\left(\frac{\partial HW}{\partial \eta}-\frac{\partial HV}{\partial \zeta}\right)\frac{\partial H}{\partial \eta}+\frac{2}{H^2}\frac{\partial H}{\partial \zeta}\frac{\partial U}{\partial Z} \quad (2)$$

Axial, Z – Momentum equation

$$\frac{W}{H}\frac{\partial U}{\partial \zeta}+\frac{V}{H}\frac{\partial U}{\partial \eta}+U\frac{\partial U}{\partial Z}=\frac{1}{H^2}\left(\frac{\partial^2 U}{\partial \zeta^2}+\frac{\partial^2 U}{\partial \eta^2}\right) \quad (3)$$

Energy equation for the fluid

$$\frac{W\partial\theta}{H\partial \zeta}+\frac{V}{H}\frac{\partial \theta}{\partial \eta}+U\frac{\partial \theta}{\partial Z}=\frac{1}{\mathrm{Pr}\,H^2}\left(\frac{\partial^2\theta}{\partial \zeta^2}+\frac{\partial^2\theta}{\partial \eta^2}\right)=0 \quad (4)$$

Integral form of the continuity equation

$$\bar{U}=\frac{8(1-N_2)}{\pi(1+N_2)}\int_0^{\pi}\int_{\eta_o}^{\eta_i} UH^2 d\eta d\zeta = 1.0 \quad (5)$$

Energy equation for each solid wall

$$\frac{\partial^2\theta_s}{\partial R^2}+\frac{1}{R}\frac{\partial\theta_s}{\partial R}+\frac{1}{R^2}\frac{\partial^2\theta_s}{\partial \phi^2}=0 \quad (6)$$

Equation (6) is applied twice, once for the outer wall with $\theta_s = \theta_{so}$ and R varying from $NR_3 = 1$ to NR_4 and then for the inner wall with $\theta_s = \theta_{si}$ and R varying from NR_1 to NR_2.

Equations (1) to (6) inclusive are subject to the following boundary conditions:

- for Z = 0 and $\eta_o < \eta < \eta_i$, V = W = P = 0 and U = 1
- for $Z \geq 0$ and $\eta = \eta_i$, U = V = W =0
- for $Z \geq 0$ and $\eta = \eta_o$, U = V = W =0
- for $Z \geq 0$ and $R = NR_1$, $\theta = 1$
- for $Z \geq 0$ and $R = NR_4$, $\theta = 0$
- for $Z \geq 0$ and $\zeta = 0$ and π (the line of symmetry)

$$\frac{\partial V}{\partial \zeta} = \frac{\partial W}{\partial \zeta} = \frac{\partial U}{\partial \zeta} = \frac{\partial \theta}{\partial \zeta} = \frac{\partial \theta_s}{\partial \phi} = 0 \tag{7}$$

The hydrodynamically fully developed flow, which occurs if the channel is sufficiently long, provides an analytical check on the numerical solution to be obtained. For this case, V = W = 0, $\partial U/\partial Z$ = 0, dP/dZ = constant, the ζ-momentum equation and the inertia terms on the left-hand side of the axial momentum equation vanish and the axial momentum equation reduces to

$$\frac{\partial^2 U_{fd}}{\partial \zeta^2} + \frac{\partial^2 U_{fd}}{\partial \zeta^2} = H^2 \left(\frac{dP}{dZ}\right)_{fd} \tag{8}$$

This equation is identical to the equation of steady-state heat conduction with internal heat generation which was solved by El-Saden (1961). The solution of this equation is

$$Ufd = A^*\eta + B - \frac{C^*}{2}\coth\eta + \sum_{n=1}^{\infty} \cos n\zeta [Ce^{n\eta} + (D - C^* \coth\eta)e^{-n\eta}] \tag{9}$$

Applying the boundary conditions, the constants of integration A*, B, C, C* and D can be determined (El-Shaarawi *et al.*, 1998).

Numerical analysis and method of solution

The six dimensionless equations listed in the previous section were expressed in finite-difference forms. A numerical algorithm has been used to solve for the three velocity components, pressure and temperature in the fluid and the temperatures in the solid cylinders. The existing computer program which was used to obtain the results reported in El-Shaarawi *et al.* (1997; 1998) has been modified to incorporate the inner and outer wall thickness and the solid-fluid conductivity ratio.

Since the governing equations for the fluid are in bipolar coordinates, whereas the energy equations for the solid walls are in cylindrical coordinates, the two grids are linked by applying the principles of the continuity of temperature (using an interpolation procedure) and the continuity of heat flux at the two interfaces.

Using backward difference to express all first derivatives with respect to Z and the first derivative of (HV) with respect to η in the continuity equation and replacing the second and other derivatives in η and ζ directions by central finite-differences, equations (1) to (6) inclusive can be written in the following forms respectively:

Continuity equation

$$\frac{H(i,j+1)W(i,j+1) - H(i,j-1)W(i,j-1)}{2\Delta\zeta} + \frac{H(i,j)V(i,j) - H(i-1,j)V(i-1,j)}{\Delta\eta} + H^2(i,j)\frac{U(i,j) - U^*(i,j)}{\Delta Z} = 0 \tag{10}$$

ζ-Momentum equation

$$\begin{aligned}
&\frac{W^*(i,j)}{H(i,j)}\frac{W(i,j+1)-W(i,j-1)}{2\Delta\zeta} \\
&+\frac{V^*(i,j)}{(H(i,j))^2}\frac{H(i+1,j)W(i+1,j)-H(i-1,j)W(i-1,j)}{2\Delta\eta} \\
U^*(i,j)&\frac{W(i,j)-W^*(i,j)}{\Delta Z}-\frac{(V^*(i,j))^2}{(H(i,j))^2}\frac{H(i,j+1)-Hi,j-1)}{2\Delta\zeta} \\
&+\frac{1}{(H(i,j))^3}\left(\begin{array}{l}\frac{H(i-1,j)W(i-1,j)-2H(i,j)W(i,j)+H(i+1,j)W(i+1,j)}{(\Delta\eta)^2} \\ +\frac{H(i,j-1)W(i,j-1)-2H(i,j)W(i,j)+H(i,j+1)W(i,j+1)}{(\Delta\zeta)^2}\end{array}\right) \\
\frac{2}{(H(i,j))^4}&\left(\frac{H(i+1,j)-H(i-1,j)}{2\Delta\eta}\right)\left(\begin{array}{l}\frac{H(i+1,j)W(i+1,j)-H(i-1,j)W(i-1,j)}{2\Delta\eta} \\ \frac{H(i,j+1)V^*(i,j+1)-H(i,j-1)V^*(i,j-1)}{2\Delta\zeta}\end{array}\right) \\
&+\frac{2}{(H(i,j))^2}\frac{H(i,j+1)-H(i,j-1)}{2\Delta\zeta}\frac{U(i,j)-U^*(i,j)}{\Delta Z}
\end{aligned} \tag{11}$$

Axial, Z – Momentum equation

$$\begin{aligned}
\frac{W^*(i,j)}{H(i,j)}\frac{U(i,j+1)-U(i,j-1)}{2\Delta\zeta}&+\frac{V^*(i,j)}{H(i,j)}\frac{U(i+1,j)-U(i-1,j)}{2\Delta\eta} \\
&+U^*(i,j)\frac{U(i,j)-U^*(i,j)}{\Delta Z} \\
&=\frac{P(i,j)-P^*(i,j)}{\Delta Z} \\
&+\frac{1}{(H(i,j))^2}\left(\begin{array}{l}\frac{U(i-1,j)-2U(i,j)+U(i+1,j)}{(\Delta\eta)^2} \\ \frac{U(i,j-1)-2U(i,j)+U(i,j+1)}{(\Delta\zeta)^2}\end{array}\right)
\end{aligned} \tag{12}$$

Energy equation for the fluid

$$\begin{aligned}
\frac{W^*(i,j)}{H(i,j)}\frac{\theta(i,j+1)-\theta(i,j-1)}{2\Delta\zeta}&+\frac{V^*(i,j)}{H(i,j)}\frac{\theta(i+1,j)-\theta(i-1,j)}{2\Delta\eta} \\
&+U^*(i,j)\frac{\theta(i,j)-\theta^*(i,j)}{\Delta Z} \\
&=\frac{1}{\mathrm{Pr}(H(i,j))^2}\left(\begin{array}{l}\frac{\theta(i-1,j)-2\theta(i,j)+\theta(i+1,j)}{(\Delta\eta)^2} \\ \frac{\theta(i,j-1)-2\theta(i,j)+\theta(i,j+1)}{(\Delta\zeta)^2}\end{array}\right)
\end{aligned} \tag{13}$$

Integral form of the continuity equation

$$\frac{8(1-NR_2)}{\pi(1+NR_2)}\left(0.5\sum_{i=2}^{N}U(i,j)(H(i,1))^2+U(i,M+1)(H(i,M+1))^2+\sum_{j=2}^{M}\sum_{i=2}^{N}U(i,j)(H(i,j))^2\right)\Delta\eta\Delta\zeta=1 \tag{14}$$

Energy equation for each solid wall

$$\frac{\theta_s(i+1,j)-2\theta_s(i,j)+\theta_s(i-1,j)}{(\Delta R)^2}+\frac{1}{[NR_*-(i-1)\Delta R]}\frac{\theta_s(i+1,j)-\theta_s(i-1,j)}{2\Delta R}+\frac{1}{[NR_*-(i-1)\Delta R]^2}\frac{\theta_s(i,j+1)-2\theta_s(i,j)+\theta_s(i,j-1)}{(\Delta\phi)^2}=0 \tag{15}$$

Equation (15) is applied for the outer wall with $\theta_s = \theta_{so}$, $NR_* = NR_4$ and also applied for the inner wall $\theta_s = \theta_{si}$, $NR_* = NR_2$.

The finite-difference equations (10) to (15) inclusive are linearized by assuming that, where the product of two unknowns occurs, one of them is given approximately by its value at the previous axial step, the variable superscripted with an asterisk (*). Moreover, backward differences are used to express all first Z-derivatives, since the equations are parabolic with respect to Z. Additionally, in the finite difference representation of the ζ-momentum equation, all the values of V have been deliberately taken at the previous axial step in order to make the equation locally (i.e. within one axial step) uncoupled from the continuity equation. Thus the finite-difference equations (10-15) represent a complete mathematical model of six equations in six unknowns (U, V, W, P, θ, and θ_s) and are numerically solved in the manner described hereafter. For the sake of symmetry, these equations need to be solved in only half the domain, i.e. for $0 \leq \zeta \leq \pi$. The variables U, V, W, θ and θ_s are computed, for a given location (Z), at the intersection of the grid lines, i.e. the mesh points.

For a fluid of a given Pr, flowing in an annulus of given NR_2 and E, the numerical solution of this set of equations is obtained by first calculating the corresponding values of η_i and η_o (El-Shaarawi *et al.*, 1998). The inner radius of the outer tube is used as reference and hence $NR_3 = 1$. By selecting the number of increments in the η and ζ directions (N and M, respectively) the values of $\Delta\eta$ and $\Delta\zeta$ can be computed. Similarly, for the solid walls, by selecting the values of NR_1 and NR_4 and the number of increments in the radial (R) and tangential (ϕ) directions (NSO, NSI and M, respectively) the values of ΔR_o, ΔR_i and $\Delta\phi$ can be determined.

Details of the numerical solution in the fluid annulus are given in El-Shaarawi *et al.* (1998). However, they are summarized hereafter. To solve for the two unknowns, P and U, at the first plane after the inlet cross-section, the

integral form of the continuity equation (14) and the finite-difference form of the axial momentum equation (12) are used. An extension to a special form of the Gauss-Jordan elimination scheme has been applied to solve the obtained matrix. The ζ-momentum equation (11) is then solved for W using Gauss-Seidel iteration and the continuity equation (10) is used to solve for V. Finally, the energy equations for the fluid (13) and solid (15) are simultaneously solved for the temperatures using Gauss-Seidel iteration. The simultaneous solution of equations (13) and (15) results in obtaining the unknown values θ, θ_{so} and θ_{si} at the second cross-section. Repeating this procedure, we proceed downstream in the Z-direction until the flow becomes fully developed.

With the boundary conditions imposed at the inner surface of the inner tube and the outer surface of the outer tube, the interface conditions are unknown. Also, the eccentric annulus is fitted with a bipolar mesh, whereas the walls have a cylindrical one resulting in 2M+2 mesh points at both the interfaces. Therefore, the three grids are linked by applying the principles of continuity of temperature and flux at four points on the intersection of the interfaces with the line of symmetry and the principle of continuity of temperature, using an interpolation procedure, at the other mesh points on the interfaces.

Results and discussion

Six controlling parameters are explicitly required to solve the problem under consideration. These are the annulus radius ratio (NR_2), the dimensionless eccentricity (E), the outer wall radius ratio (NR_4), the inner wall radius ratio (NR_1), the solid-fluid conductivity ratio (KR), the Prandtl number (Pr). It is worth mentioning that the eccentricity e can vary from zero to a maximum value of ($r_{io} - r_{oi}$) = $D_h/2$. Thus the dimensionless eccentricity E can vary from zero to unity. Computations were carried out for a fluid of Pr = 0.7 in an annulus of radius ratio $NR_2 = 0.5$ with $NR_4 = 1.2$ and $NR_1 = 0.4$ for values of E = 0.1, 0.3, 0.5 and 0.7 and KR = 1, 10, 50, 100 and 1,000. The reason for the selection of $NR_2 = 0.5$ is that most of the results in the literature for the conventional problem (i.e. neglecting the effect of conjugation) are reported for this particular value, which represents a typical annular geometry. Only one value of Pr = 0.7 has been selected due to space limitations and since it represents air. The selected values of NR_4 and NR_1 are typical practical values, as can be seen from Table I, which lists some values of radius ratios for possible combination of inner/outer standard steel pipes. Table II indicates practical values of the solid fluid conductivity ratio (KR) and displays the widest possible range.

To check the adequacy of the present computer code, special runs were made with very large values of KR and very thin walls. For a typical large value of solid-fluid conductivity ratio (KR) = 1,000 and very thin walls corresponding to $NR_1 = 0.499$, $NR_2 = 0.5$ and $NR_4 = 1.002$, the results of the present computer code with E = 0.5 and 0.6, for the fully developed heat transfer parameters, are in excellent agreement with the conventional case results (Trombetta, 1972; Feldman *et al.*, 1982b; El-Shaarawi *et al.*, 1998). The maximum deviation between the present results and those of Trombetta (1972), Feldman *et al.* (1982b) and El-Shaarawi *et al.* (1998) are 0.3 percent, 1.4 percent and 0.05 percent, respectively.

Nominal size (inch) Inner	Outer		Radius ratios NR_1	NR_2	NR_4	Dimesionless tube thickness Inner	Outer
$\frac{1}{4}$	1	SCH. 40	0.35	0.51	1.25	0.17	0.25
		SCH. 80	0.32	0.56	1.37	0.25	0.37
$\frac{3}{8}$	1 1/4	SCH. 40	0.36	0.49	1.20	0.13	0.20
		SCH. 80	0.33	0.53	1.30	0.20	0.30
$\frac{1}{2}$	1 1/2	SCH. 40	0.39	0.52	1.18	0.14	0.18
		SCH. 80	0.36	0.56	1.27	0.20	0.27
$\frac{3}{4}$	2	SCH. 40	0.40	0.51	1.15	0.11	0.15
		SCH. 80	0.38	0.54	1.22	0.16	0.22
1	2 1/2	SCH. 40	0.42	0.53	1.16	0.11	0.16
		SCH. 80	0.41	0.57	1.24	0.15	0.24
1 $\frac{1}{2}$	4	SCH. 40	0.40	0.47	1.12	0.07	0.12
		SCH. 80	0.39	0.50	1.18	0.10	0.18

Table I.
Radius ratios for standard steel pipes

Material	Ther. conductivity (W/M-DEG.C)
Air @ 300K	0.02624
Carbon steel (1 % C)	43
Water-saturated @ 300K	0.613
Cast iron (4 % C) @ 293K	52
Engine oil (SAE 50) @ 293K	0.145
Aluminium metal @ 293K	236
Asbestos @ 273K	0.154
Plastic	0.48

Solid-fluid conductivity ratio – KR

	Air	Water	Oil
Aluminium	8993.90	384.99	1627.59
Cast iron	1981.71	84.83	358.62
Steel	1638.72	70.15	296.55
Plastic	18.29	0.78	3.31
Asbestos	5.87	0.25	1.06

Table II.
Common values of KR

Moreover, results obtained by setting E = 0.01 with the above-mentioned values of KR and NR_4 but with $NR_1 = 0.249$ and $NR_2 = 0.25$, are in good agreement with the conventional solutions for the concentric case, as reported in the literature (Shah and London, 1978); the maximum deviation is about 2 percent. Tables III and IV give comparisons between the present numerical solutions and other corresponding conventional solutions available in the literature.

Results have been obtained using a grid of 20 segments in each of the η and ζ directions in the fluid annulus. For the solid walls, 20 segments were used in the tangential (ϕ) direction with 16 and eight segments in the radial (R) direction for the outer and inner walls respectively; the outer tube thickness being taken as twice that of the inner one. At 20 percent CPU share, the time required for one run

Results of Shumway and McEligot as reported by Shah and London (1978)

	HFI		HFO		θ_m	
Z^*	(Shah and London, 1978)	Present	(Shah and London, 1978)	Present	(Shah and London, 1978)	Present
0.01	8.05	7.555	0.0088	0.0227	0.0948	0.1041
0.05	5.31	5.268	0.641	0.6606	0.2533	0.2579
0.1	4.567	4.566	0.9735	0.977	0.312	0.3142
	NUII		NUOI			
Z^*	(Shah and London, 1978)	Present	(Shah and London, 1978)	Present		
0.01	8.892	8.432	0.0936	0.2179		
0.05	7.112	7.098	2.53	2.562		
0.1	6.639	6.658	3.12	3.109		

Fully developed axial pressure gradient (DPDZFD)

(Shah and London, 1978)	Present		
	Analytical	Numerical	
46.604	46.917	45.983	

Results of Lundberg *et al.* and Worse-Schmidt as reported by Shah and London (1978)

HFIFD		NUIFD		NUOFD		$\theta_{m,fd}$	
(Shah and London, 1978)	Present	(Shah and London, 1978)	Present	(Shah and London, 1978)	Present	(Shah and London, 1978)	Present
4.328	4.414	6.471	6.553	3.267	3.204	0.3312	0.3264

HFI Heat flux on the inner interface
HFO Heat flux on the outer interface
NUII Nusselt number on the inner interface
NUOI Nusselt number on the outer interface
θ_m Mixed-mean temperature
$\theta_{m,fd}$ Fully developed mixed-mean temperature
HFIFD Fully developed value of HFI
NUIFD Fully developed value of NUII
NUOFD Fully developed value of NUOI

Table III.
Comparisons with available conventional solutions for concentric annuli, $NR_1 = 0.249$, $NR_2 = 0.25$; $NR_4 = 1.002$; KR = 1,000; E = 0.01; Pr = 0.72

Results of Tiedt as reported by Shah and London (1978) for E = 0.6, Pr = 0.7

DPDZFD		
Tiedt	Present	
	Analytical	Numerical
31.818	31.963	32.207

Results of Trombetta (1972) for E = 0.6; Pr = 0.7

HFIFD		NUIFD		NUOFD	
Trombetta	Present	Trombetta	Present	Trombetta	Present
3.582	3.593	5.746	5.738	4.754	4.762

Results of Feldman *et al.* (1982b) for E = 0.5; Pr = 1.0

DPDZFD		
Feldman *et al.*	Present	
	Analytical	Numerical
35.34	35.49	35.73

θm,fd		NUIFD		NUOFD	
Feldman *et al.*	Present	Feldman *et al.*	Present	Feldman *et al.*	Present
0.3848	0.3793	5.39	5.383	4.308	4.318

	θm		NUII		NUOI	
Z*	Feldman *et al.*	Present	Feldman *et al.*	Present	Feldman *et al.*	Present
0.001	0.0362	0.0416	13.08	15.119	0.00042	0.00008
0.01	0.1319	0.1526	6.858	7.668	3.46	1.537
0.1	0.3209	0.3517	5.184	5.35	4.601	4.334

HFI	Heat flux on the inner interface
HFO	Heat flux on the outer interface
NUII	Nusselt number on the inner interface
NUOI	Nusselt number on the outer interface
θ_m	Mixed-mean temperature
$\theta_{m,fd}$	Fully developed mixed-mean temperature
HFIFD	Fully developed value of HFI
NUIFD	Fully developed value of NUII
NUOFD	Fully developed value of NUOI

Table IV.
Comparisons with available results for eccentric annuli, NR_1 = 0.499; NR_2 = 0.5; NR_4 = 1.002; KR = 1,000

was about two hours and a half on an IBM RISC mainframe computer with AIX operating system. The machine has a RAM of 256MB and speed 71.5MHz. With a finer mesh, N = M = 30, the time increased eightfold, requiring about 24 hours at the same CPU share. However, the difference in the values of the results for the two mesh sizes was not significant (maximum 3 percent) and therefore the former mesh (N = M = 20) was used for all computations. On the other hand, since very large gradients exist near the entrance, computations were made with very small axial steps near the entrance $\Delta Z = 10^{-10}$), with the axial step size being gradually increased several times as the flow moves downstream to reach a maximum value of $\Delta Z = 10^{-3}$ near full development.

It is worth mentioning that the higher the Peclet number, the more valid is the assumption of no axial direction heat transfer in the solid. The reader may refer to a paper by Schmidt and Zeldin (1970) in this context.

Owing to space limitations, only a representative sample of the results will be shown here. Figures 3 and 4 show the developing temperature profile, corresponding to different values of Z, across the narrowest and the widest gaps, respectively for KR = 10 and E = 0.5. It is noticed that full development is reached significantly faster across the narrowest gap (Z = 0.0832) compared with the widest gap (Z = 0.203). This is expected because the eccentricity leads to a reduced overall resistance across the narrowest gap, resulting in the heat signal being sensed relatively earlier.

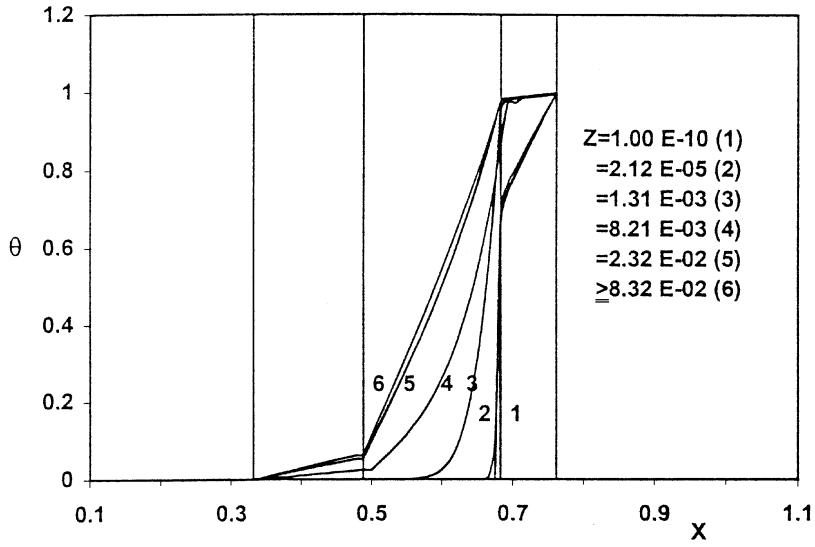

Figure 3.
Developing temperature profiles across the narrowest gap. E = 0.5, KR = 10, NR_1 = 0.4, NR_2 = 0.5 and NR_4 = 1.2

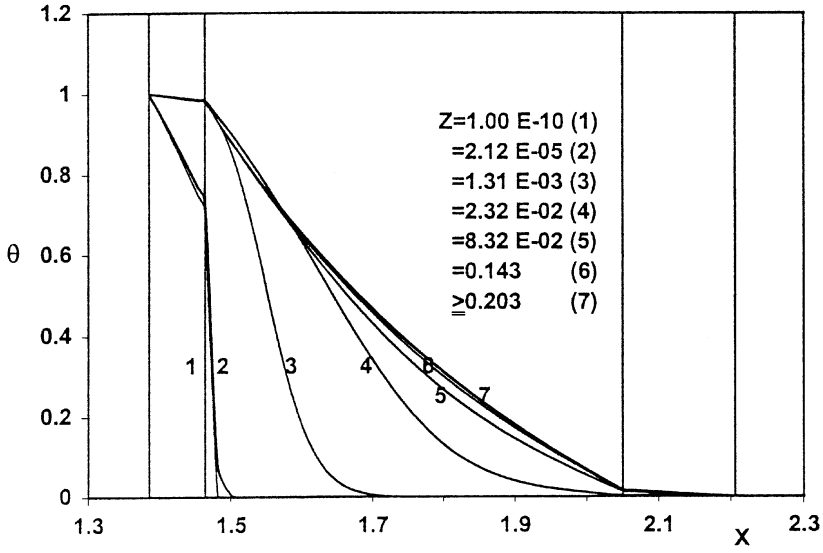

Figure 4.
Developing temperature profiles across the widest gap. E = 0.5, KR = 10, NR_1 = 0.4, NR_2 = 0.5 and NR_4 = 1.2

Each pair of Figures 5-8 displays the variation with KR, of the fully developed temperature profile across the narrowest and the widest gaps in the same annulus ($NR_1 = 0.4$, $NR_2 = 0.5$ and $NR_4 = 1.2$) but for E = 0.3 and E = 0.5, respectively. It is obvious that increasing the value of KR results in a smaller temperature drop across the solid walls. The effect of increasing eccentricity is a steeper temperature profile across the narrowest gap and a flatter one across the widest gap.

Figures 9 and 10 give the variation with eccentricity, at KR = 10, of the fully developed circumferential temperature distribution at the outer and the inner interfaces respectively. The figures indicate how the increase in the value of the eccentricity enhances the circumferential variation of temperature. The

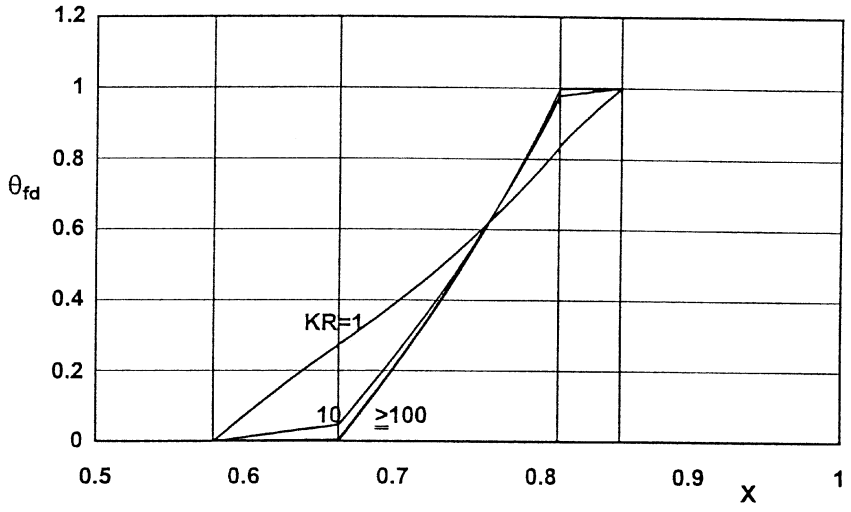

Figure 5.
Variation with KR of the fully developed temperature profile across the narrowest gap. E = 0.3, $NR_1 = 0.4$, $NR_2 = 0.5$ and $NR_4 = 1.2$

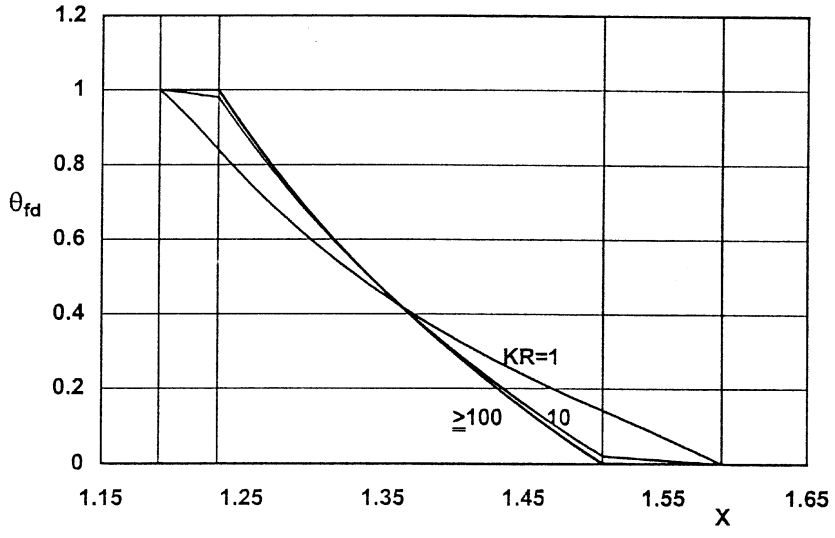

Figure 6.
Variation with KR of the fully developed temperature profile across the widest gap. E = 0.3, $NR_1 = 0.4$, $NR_2 = 0.5$ and $NR_4 = 1.2$

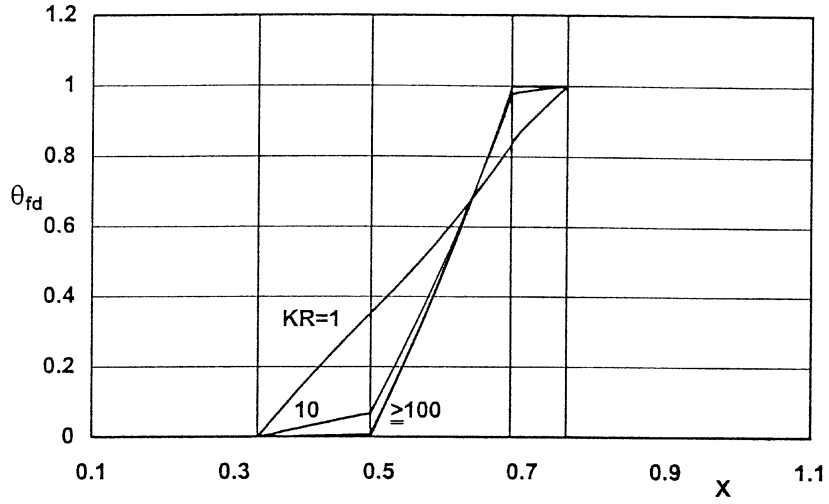

Figure 7.
Variation with KR of the fully developed temperature profile across the narrowest gap. E = 0.5, NR_1 = 0.4, NR_2 = 0.5 and NR_4 = 1.2

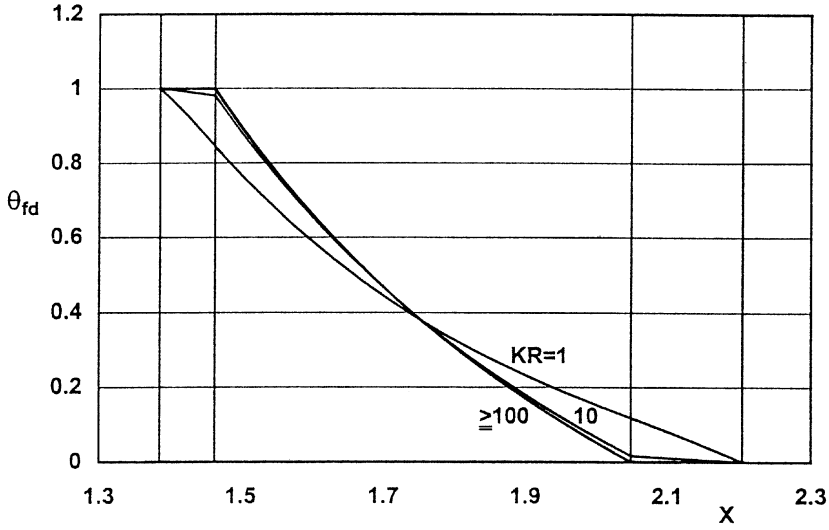

Figure 8.
Variation with KR of the fully developed temperature profile across the widest gap. E = 0.5, NR_1 = 0.4, NR_2 = 0.5 and NR_4 = 1.2

increased circumferential temperature variation at the interfaces results in increased deviation from the conventional case with isothermal boundaries; thus consideration of conjugation is more important at higher eccentricities. It can be observed from Figures 9 and 10 that the higher the value of E, the higher the temperature at the narrowest gap (ψ = 1) on the outer interface and at the widest gap (ψ = 0) on the inner interface. Moreover, the higher the value of E, the higher the circumferential variation of temperature on either interface (i.e. higher circumferential temperature gradient). Consequently, the higher the value of E, the larger the circumferential heat flow. The circumferential heat

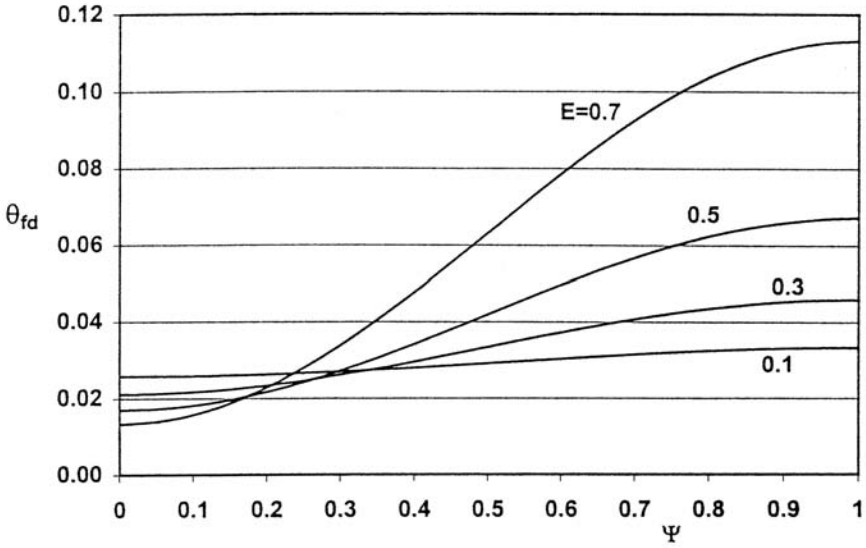

Figure 9.
Variation with eccentricity of the fully developed circumferential temperature distribution at the outer interface. KR =10, NR_1 = 0.4, NR_2 = 0.5 and NR_4 = 1.2

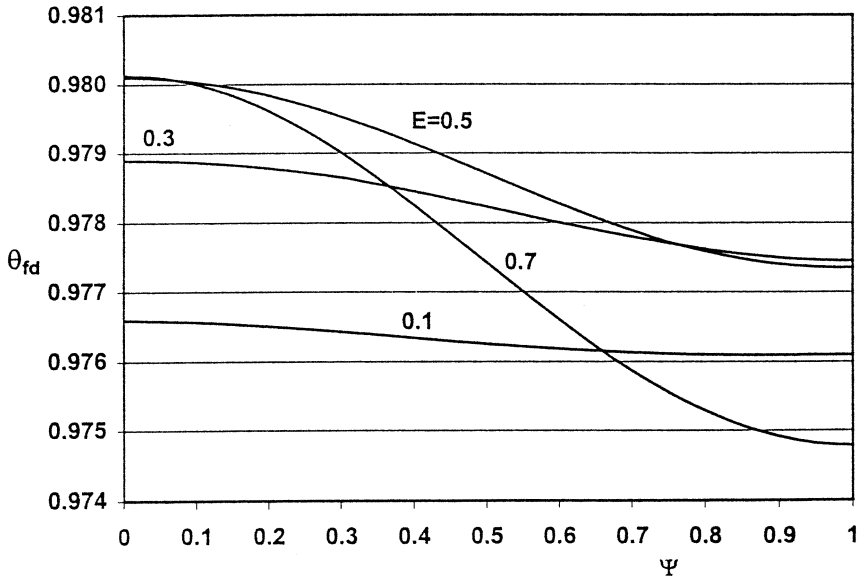

Figure 10.
Variation with eccentricity of the fully developed circumferential temperature distribution at the inner interface. KR =10, NR_1 = 0.4, NR_2 = 0.5 and NR_4 = 1.2

flow on the inner interface is in the positive ζ-direction (i.e. from the widest to the narrowest gap side). However, it is in the opposite direction (the negative ζ-direction) on the outer interface.

Figures 11 and 12 show the effect of KR (at E = 0.5) and eccentricity (at KR = 10) respectively, on the axial distribution of the peripherally averaged heat flux on the inner interface. Figure 11 indicates that increasing KR results in increased heat flux, approaching almost exactly the values of the conventional case at KR =

100 (with a maximum deviation of 0.5 percent based on the conventional case results). Figure 12 highlights that heat flux increases with increasing eccentricity.

Engineers are not frequently concerned with the temperature profiles but with the mixed-mean (mixing-cup) temperature. The importance of the mixed-mean temperature comes from the fact that it can be directly used to obtain the heat gained by the fluid. Figures 13 and 14 present the variation with KR and eccentricity, respectively, of the axial distribution of the mixing-cup temperature θ_m.

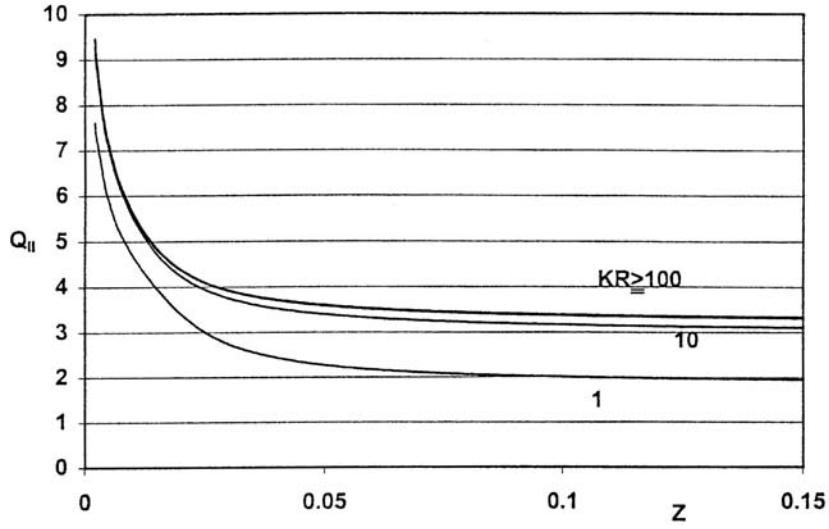

Figure 11.
Variation with KR of the axial distribution of the circumferentially averaged heat flux at the inner interface. E = 0.5, NR_1 = 0.4, NR_2 = 0.5 and NR_4 = 1.2

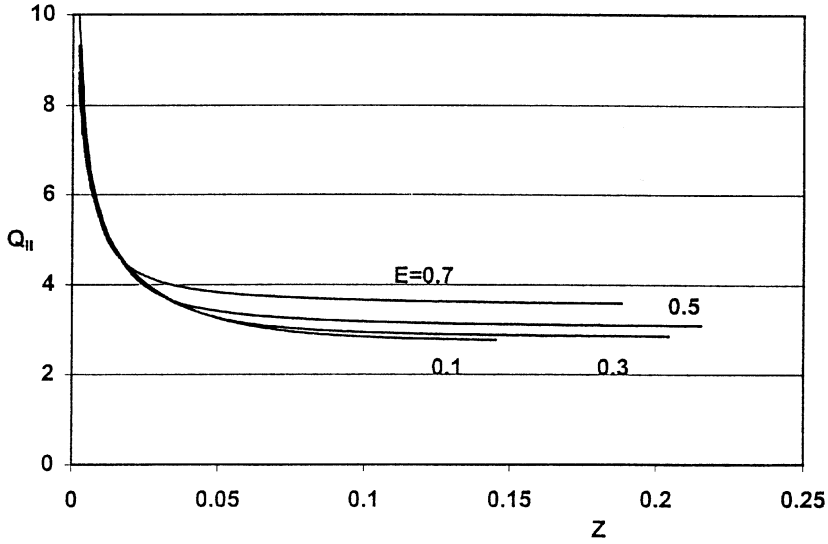

Figure 12.
Variation with eccentricity of the axial distribution of the circumferentially averaged heat flux at the inner interface. KR = 10, NR_1 = 0.4, NR_2 = 0.5 and NR_4 = 1.2

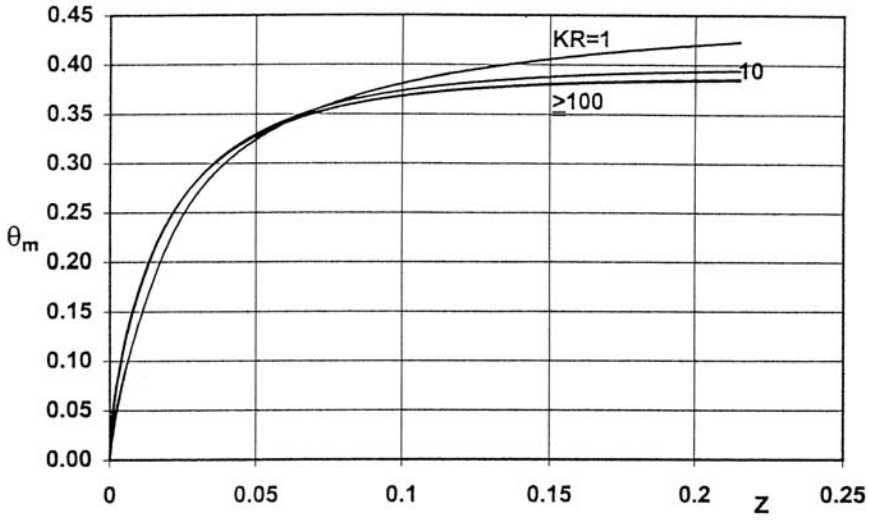

Figure 13.
Variation with KR of the axial distribution of the mixing-cup temperature. E = 0.5, NR_1 = 0.4, NR_2 = 0.5 and NR_4 = 1.2

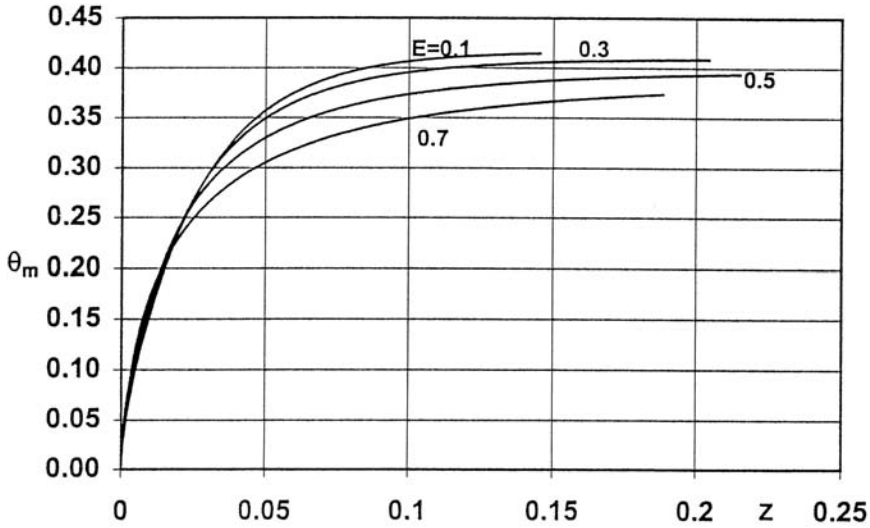

Figure 14.
Variation with eccentricity of the axial distribution of the mixing-cup temperature. KR = 10, NR_1 = 0.4, NR_2 = 0.5 and NR_4 = 1.2

Away from the entrance, the lower values of θ_m and higher values of KR in Figure 13 indicate increased local heat flux due to reduced wall resistance. This is because the local heat flux is directly proportional to the difference between the wall temperature and the fluid mixed-mean temperature ($Q \propto (\theta_w - \theta_m)$). Consequently, with an isothermal boundary ($\theta_w = 1$), the increase in the value of θm will cause a decrease in the local value of the wall heat flux (Q). However, it can be noticed that near the entrance the trend is reversed, i.e. the higher the value of KR, the higher the value of θ_m. The reason for this is that near the entrance the increase in the value of KR results in more heat being gained by

the fluid through the isothermally heated surface than that lost by the fluid through the wall maintained at the ambient temperature. The increase in the heat gained by the fluid near the entrance through the heated boundary is attributed to the presence of the radial-like (η) and tangential-like (ζ) velocity components. These two velocity components decay as the flow moves away from the entrance and hence the reverse phenomenon occurs, as explained before. Moreover, near the entrance, the fluid near the outer wall has not sensed the heat signal and is still at the ambient temperature, resulting in no heat loss through the outer ambient wall. As the flow moves downstream, heat loss through the outer wall initiates due to the rise in the fluid temperature.

For a given value of KR (KR = 10), Figure 14 presents the axial variation of θ_m for various values of E. As can be seen from this figure, for a given Z, the higher the value of E, the lower the value of θ_m. The decrease in the value of θ_m with E is attributed to the increase in the mass flow rate through the annulus.

Finally, it is of practical importance to know the value of KR beyond which the conjugate effect can be neglected. Figure 15 shows graphically the results of the present investigation for the percent difference variation in $\theta_{m,fd}$ from the conventional case with KR and E. This percent difference is based on the conventional values of $\theta_{m,fd}$. The "critical" value of KR for a given eccentricity has been arbitrarily chosen as that value which causes $\theta_{m,fd}$ to differ by no more than 1 percent from the conventional solution result for a given eccentricity. According to this criterion, the critical values of KR are also presented in Table V. As can be seen from this table, the higher the value of E, the higher the critical KR. Thus it can be concluded that the effect of conjugation increases with eccentricity.

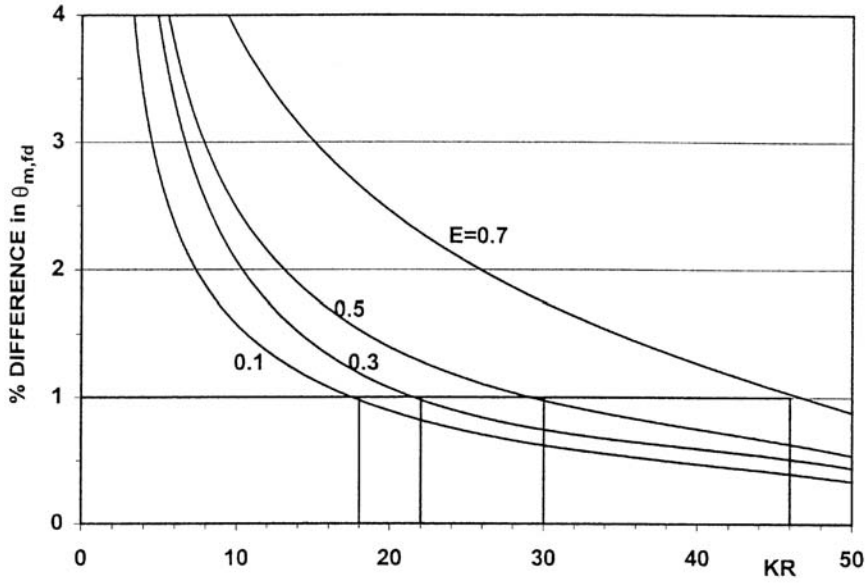

Figure 15.
Percentage difference in $\theta_{m,fd}$ from the conventional case plotted against solid-fluid conductivity ratio (KR) for various values of E. Critical KR values for a 1 percent difference are highlighted

	Fully developed mixing-cup temperature ($\theta_{m,fd}$)			
KR	E = 0.1	E = 0.3	E = 0.5	E = 0.7
1	0.433904678	0.438773572	0.423074216	0.402607769
percent diff.	6.25	9.53	10.02	11.79
10	0.41480425	0.40887475	0.394055575	0.374003261
percent diff.	1.57	2.06	2.47	3.85
50	0.409776419	0.402387351	0.386617273	0.363301039
percent diff.	0.34	0.44	0.54	0.88
100	0.409090549	0.401506364	0.385590166	0.361745119
percent diff.	0.17	0.22	0.27	0.44
1,000	0.408467799	0.400699079	0.384645969	0.360298812
percent diff.	0.02	0.02	0.03	0.04
Infinity	0.408396483	0.400613785	0.384539783	0.360143453
θm (percent)	0.412480447	0.404619923	0.388385181	0.363744887
Critical KR	18	22	30	46
θm @ CKR	0.412098229	0.404556871	0.387951374	0.363566339
percent diff.	0.91	0.98	0.89	0.95

Table V.
Critical solid-fluid conductivity ratio (KR)

However, Figure 15 can also be used to obtain critical KR values for other percent difference criteria. Moreover, for given E and KR, this diagram can be useful in correcting available conventional results to take into account the effect of conjugation.

Conclusions

The present work was aimed at obtaining a solution for the conjugate laminar forced convection heat transfer in the entry region of eccentric annuli. Thermal boundary conditions applied are isothermal heating of the inner surface of the inner tube while the outer surface of the outer tube is maintained at the inlet fluid temperature. A model using bipolar grid to fit the eccentric annulus and cylindrical grids in the walls has been presented. A linearized finite-difference algorithm has been developed to solve the model equations which comprise the continuity equation, the axial and tangential-like momentum equations and the fluid and solid energy equations.

Numerical results are presented for a fluid of Pr = 0.7 flowing in an annulus of radius ratio 0.5 for four values of dimensionless eccentricity. The solid-fluid conductivity ratio (KR) was varied to cover the range for typical practical cases with standard tube thickness. The numerical results indicate that conjugation can have an appreciable effect on the heat transfer parameters and that this effect increases with increasing eccentricity. Thus, taking this into consideration, the conjugation is more important at higher eccentricities. Based on the results of this investigation, limits have been determined for the solid-fluid conductivity ratio, above which conjugation can be neglected for practical purposes.

References

Caldwell, J. (1930), "The hydraulic mean depth as a basis for form comparison in the flow of fluids in pipes", *J.R. Tech. Coll*, Glasgow, Vol. 2, pp. 203-20.

Cheng, K.C. and Hwang, G.J. (1968), "Laminar forced convection in eccentric annuli", *A.I.Ch.E. Journal*, Vol. 14 No. 3, pp. 510-12.

El-Saden, M.R. (1961), "Heat conduction in an eccentrically hollow, infinitely long cylinder with internal heat generation", *Journal of Heat Transfer*, Vol. 83, pp. 510-12.

El-Shaarawi, M.A.I., Abualhamayel, H.I. and Mokheimer, E.M.A. (1997), "Developing laminar flow in eccentric annuli", *Journal of Fluids Engineering, Transactions of the ASME*, Vol. 119, pp. 724-8.

El-Shaarawi, M.A.I., Abualhamayel, H.I. and Mokheimer, E.M.A. (1998), "Developing laminar forced convection in eccentric annuli", *Heat and Mass Transfer*, Vol. 33, pp. 353-62.

Faghri, M. and Sparrow, E.M. (1980), "Simultaneous wall and fluid axial conduction in laminar pipe-flow heat transfer", *Journal of Heat Transfer*, Vol. 102, pp. 58-63.

Feldman, E.E., Hornbeck, R.W. and Osterle, J.F. (1982a), "A numerical solution of laminar developing flow in eccentric annular ducts", *International Journal of Heat and Mass Transfer*, Vol. 25 No. 2, pp. 231-41.

Feldman, E.E., Hornbeck, R.W. and Osterle, J.F. (1982b), "A numerical solution of temperature for laminar developing flow in eccentric annular ducts", *International Journal of Heat and Mass Transfer*, Vol. 25 No. 2, pp. 243-53.

Kirshan, B. (1983), "On conjugated heat transfer in fully developed flow", *International Journal of Heat and mass Transfer*, Vol. 30, pp. 288-9.

Mori, S., Inoue, T. and Tanimoto, A. (1978), "Heat transfer to laminar flow between parallel plates with interfacial heat generation", *Journal of Chemical Engineering*, Vol. 11, Japan, pp. 83-8.

Mori, S., Kawamura, Y. and Tanimoto, A. (1979), "Conjugated heat transfer to laminar flow with internal heat source in a parallel plate channel", *The Canadian Journal of Chemical Engineering*, Vol. 57, pp. 698-703.

Olek, S., Ellias, E., Wacholder, E. and Kaizerman, S. (1991), "Unsteady conjugated heat transfer in laminar pipe flow", *International Journal of Heat and Mass Transfer*, Vol. 34, pp. 1443-50.

Pagliarini, G. (1991), "Conjugate heat transfer for simultaneously developing laminar flow in a circular tube", *Journal of Heat Transfer*, Vol. 113, pp. 763-6.

Piercy, N.A.V., Hooper, M.S. and Winny, H.F. (1933), "Viscous flow through pipes with cores", *Philos. Mag. J. Sci*., Vol. 15, London-Edinburgh-Dublin, pp. 647-76.

Redberger, P.J. and Charles, M.E. (1962), "Axial laminar flow in a circular pipe containing a fixed eccentric core", *The Canadian Journal of Chemical Engineering*, pp. 148-51.

Sakakibara, M., Mori, S. and Tanimoto, A. (1987), "Conjugate heat transfer with laminar flow in an annulus", *The Canadian Journal of Chemical Engineering*, Vol. 65, pp. 541-9.

Sathymurthy, P., Karki, K.C. and Patankar, S.V. (1992), "Laminar fully developed mixed convection in a vertical eccentric annulus", *Numerical Heat Transfer*, Part A, Vol. 22, pp. 71-85.

Schmidt, F.W. and Zeldin, B. (1970), "Laminar heat transfer in the entrance region of ducts", *Applied Scientific Research*, Vol. A23, pp. 73-94.

Shah, R.K. and London, A.L. (1978), *Laminar Flow Forced Convection in Ducts*, Academic Press, New York, NY.

Snyder, W.T. and Goldstein, G.A. (1965), "An analysis of a fully developed laminar flow in an eccentric annulus", *A.I. Ch. E. Journal*, Vol. 11 No. 3, pp. 462-9.

Suzuki, K., Szmyd, J.S. and Ohtsuka, H. (1990), "Laminar forced convection heat transfer in eccentric annuli", originally published in *Trans. J. ASME*, Vol. 56, pp. 3445-50.

Trombetta, M.L. (1972), "Laminar forced convection in eccentric annuli", *International Journal of Heat and Mass Transfer*, Vol. 14, pp. 1161-72.